Seeding Effectiveness—The Interaction of Desert Dust and the Southern Margins of Rain Cloud Systems in Israel

DANIEL ROSENFELD AND RONIT NIREL

Hebrew University of Jerusalem, Jerusalem, Israel

(Manuscript received 7 November 1994, in final form 12 February 1996)

ABSTRACT

Statistical analyses suggest that cloud seeding has caused a net increase of rainfall only in northern Israel. These analyses also identify the reported desert dust as a detrimental factor for the seeding effectiveness. This paper deals with the question of what role the interaction of desert dust and the dynamic properties of the clouds plays in the determination of divergent seeding effects in Israel.

This question is investigated through analyses of the cloud seeding effectiveness in northern Israel (Israel-2 experiment and the operational seeding) stratified into days when the southern margins of the rain cloud system (SMR) locations were in the north or in the south and into "dust" and "no-dust" days.

The results indicate that the SMR plays an important role on dust days, where a seeding effect of 11% is indicated on days with the SMR in the south, and an effect of −11% is indicated on days with the SMR in the north. On no-dust days positive effects were indicated regardless of the location of the SMR. These results are consistent with the following observations.

- The strongest interaction of desert dust with rain clouds in the north occurs on dust days when the SMR is in the north.
- When the SMR moves to the south, much of the desert dust is washed down by the intervening rain between the north and the SMR.

1. Introduction

a. The objective of this study

Analysis of the typical dynamic structure of the lower troposphere during rain situations in Israel shows the potential for major interaction between the southern margins of the rain cloud system (SMR) and the dust bearing air masses to their south. The SMR typically resides in the southern target area of the Israel-2 experiment, which later became the target area of the Israel-3 experiment, where no overall rain enhancement was obtained. It is the objective of this paper to deal with the question of what role the interaction of desert dust and the dynamic properties of the clouds plays in the determination of divergent seeding effects in Israel. This question is investigated through analysis of the divergent seeding effects in northern Israel in the period 1969/70–1990/91.

b. The Israeli rain enhancement project

In Israel AgI cloud seeding is conducted at cloud base along a seeding line parallel to the coastline, upwind of the target areas. Seeding is performed during both day and night provided the appropriate conditions exist.

Rain enhancement experiments in Israel started with the crossover Israel-1 experiment (1960/61–1966/67), which indicated an overall increase of 15% in rain amounts. (Gagin and Neumann 1974). The subsequent Israel-2 experiment (1969/70–1974/75) indicated a significant seeding effect of 13% in the northern part of Israel and a nonsignificant overall effect of −2.5% in the crossover analysis of the north and south (Gagin and Neumann 1981; Gabriel and Rosenfeld 1990). Since November 1976, the Israel-3 experiment has been carried out in the southern part of the country, while in the north seeding is operational. The northern target and control areas of the operational project are similar to those of Israel-2 and are indicated by NT (northern target) and NC (northern control) in Fig. 1. Analyses of the operational seeding in the north showed statistically significant rain enhancement between 7% and 11% (Nirel and Rosenfeld 1995). The southern target area of Israel-3 is composed of the two subareas SN and SS in Fig. 1, and the southern control area is SC. Preliminary results of Israel-3 indicate no overall effect in the south (Nirel and Rosenfeld 1994).

c. The ice nucleating activity of desert dust

Desert dust has already been found to be active as ice nuclei (IN) at temperatures colder than −11°C by

Corresponding author address: Dr. Daniel Rosenfeld, Atmospheric Sciences, Hebrew University of Jerusalem, Jerusalem 91904, Israel.
E-mail: daniel@vms.huji.ac.il

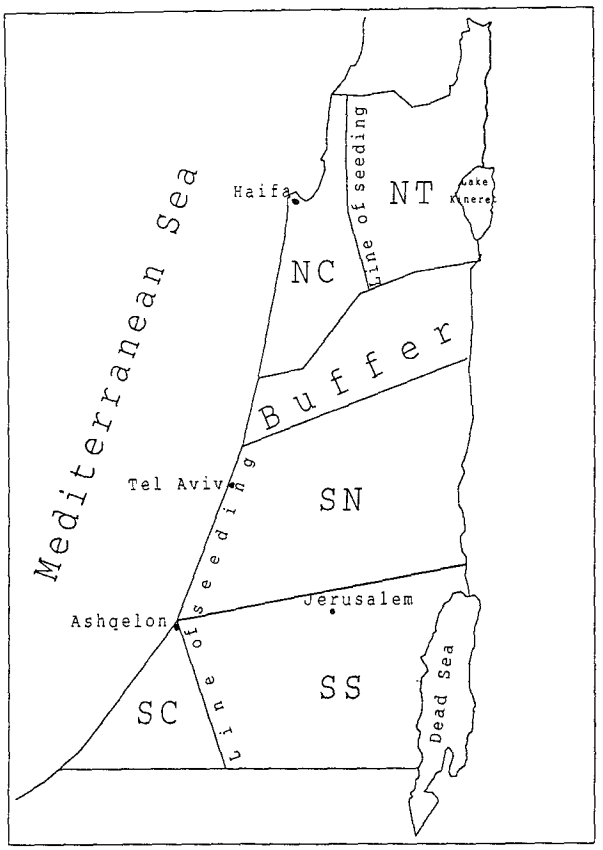

FIG. 1. Map of the Israeli cloud seeding projects for rain enhancement: north control (NC), north target (NT), south control (SC), and two subareas of the southern target, (SN) and (SS).

Schaefer (1949, 1954). The ice nuclei in the desert dust are mainly clay minerals (Isono et al. 1959). Gagin (1965) and Levi and Rosenfeld (1996) have shown that desert dust in Israel, brought by southwesterly winds from the Sahara, has ice nucleating activity similar to that found by Schaefer. Ganor (1991) showed that the minerals in the dust (illite and kaolinite) are those that, according to the other studies, explain the ice nucleating activity of the desert dust transported to Israel.

d. *The cloud condensation nucleating activity of desert dust*

Desert dust in Israel often contains large amounts of soluble material, which can serve as cloud condensation nuclei (CCN). Levin et al. (1990) found that particles of desert dust are coated with sulfates. The amount of soluble material on the dust particles can be large enough to nucleate large cloud droplets, which can accelerate the processes of coalescence between cloud droplets. This enhanced coalescence can lead to the formation of warm rain—that is, rain formation without the ice phase (Levin et al. 1996a). The existence of cloud droplets with diameters greater than 25 μm is conducive to ice multiplication much beyond the number of ice nuclei in the cloud (Hallet and Mossop 1974). Numerical simulations (Levin et al. 1996b) show that other microphysical mechanisms as well can cause the enhancement of ice formation in clouds with large droplets, such as may be caused by the desert dust.

e. *The desert dust as a natural "cloud seeder"*

The effects of dust on rain enhancement should be viewed with respect to the conceptual model of "static seeding" in Israel, which postulates the following.

- The liquid water in clouds is mostly found in drops that are too small to precipitate during the limited lifetime of the cloud. As ice is formed at temperatures below 0°C, the cloud becomes thermodynamically unstable, and ice crystals rapidly grow to precipitation-sized particles by deposition, at the expense of the evaporating drops, or by aggregation with drops or other ice crystals.
- In some of the clouds, the natural concentration of ice particles is less than optimal for the most efficient conversion of cloud water into precipitation.
- Seeding such clouds with ice nuclei, usually in the form of AgI, creates more ice crystals, which produces more precipitation.

Both ice and condensation nucleating activities of the desert dust can enhance the natural ice in the cloud to amounts approaching or exceeding the concentrations required for optimal precipitation efficiency. In such cases, artificial addition of ice by AgI seeding cannot enhance the rainfall.

Recent measurements of cloud droplet spectra in Israel showed that ice multiplication conditions (Hallet and Mossop 1974) exist. This enhances the impact of IN on the timing of cloud glaciation by the mechanism of ice multiplication. In such a situation, the IN concentration for optimal precipitation may by much lower than the concentration induced by "static seeding," which then would result in "overseeding."

f. *The "dust index"*

Rosenfeld and Farbstein (1992) have suggested that the large difference in the seeding effect between northern and southern Israel is due to the higher occurrence of desert dust in the south. They suggested that in the presence of dust, the static seeding hypothesis may be invalidated. They have also suggested that the dust serves as ice nuclei and/or giant CCN, facilitating warm rain and ice multiplication processes. The only historically available data related to the background of natural aerosols in Israel are the dust and dust storms observations in the regular synoptic reports. Rosenfeld

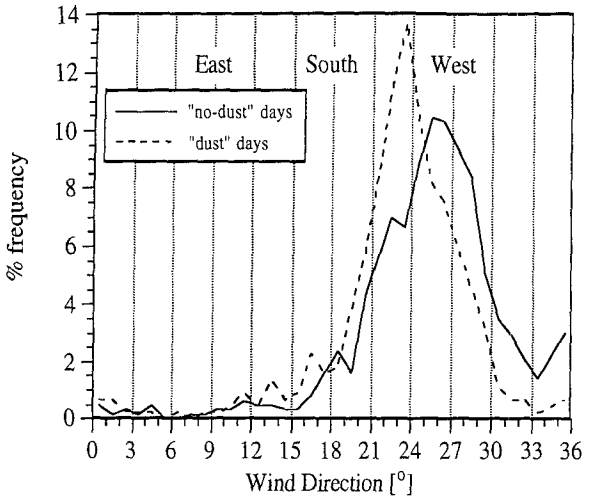

FIG. 2. Frequency of wind directions at the level of 850 mb near Tel Aviv during 438 dust and 630 no-dust rain days in Israel. The abscissa is azimuth/10.

and Farbstein (1992) used these reports to define a dust index as follows.

- "Dust" day: A day in which at least 1 of 14 synoptic meteorological stations in central and southern Israel reported weather conditions of "dust" or "sand storm" at least once.
- "No-dust" day: A day in which no dust or dust storm was reported by any of these stations.

The dust index was defined by stations in central and southern Israel because the rainfall in the north often masked the possibility of observing the "dust haze."

The relevance of this crude dust index to the desert dust and background IN concentration was investigated by Levi and Rosenfeld (1996), who have shown evidence that the average concentrations of IN in central Israel were doubled in dust days as compared to the no-dust days. The difference was statistically significant.

g. *Statistical relationships between desert dust and rain enhancement*

Statistical analyses of the Israel-2 experiment (Rosenfeld and Farbstein 1992), the Israel-3 experiment, and the operational seeding (Nirel and Rosenfeld 1994) have shown that the presence of atmospheric desert dust is the most important factor found to date that can explain the wide variability of the seeding effects in Israel.

Large and statistically significant rain enhancement was achieved during no-dust days in northern Israel (24% in Israel-2 and 12% in the operational seeding), while zero to statistically insignificant results were obtained there during dust days (−2% in Israel-2 and 6% in the operational seeding). Similar differential effects were obtained in the south, but with lower overall seeding effects (5% in no-dust days and −6% in dust days of Israel-3).

These results are consistent with the physical evidence of high rainwater salinity of continental origin and of high ice nuclei concentrations when seeding was found to be less effective (Levi and Rosenfeld 1996).

h. *The southern origin of the desert dust*

Rainfall in Israel is brought mostly by westerly to southwesterly lower-tropospheric winds. The most frequent wind direction during no-dust days is just westerly, while the winds in dust days are mostly from the southwest. This is illustrated in Fig. 2, which presents a histogram of 850-mb wind directions near Tel Aviv, Israel, during 1068 rain days, divided into 438 dust and 630 no-dust days. According to Fig. 2, even though dust occurred mostly with southwesterly winds, many of the days with 850-mb westerly winds were designated dust days.

Chemical analyses of rainwater showed that all days with high calcium content in the north were accompanied by at least an equally high calcium content in the south, while the opposite was not true (Fig. 3). Almost all the calcium in the rainwater (98%) is of continental origin, mainly from desert dust (Levi and Rosenfeld 1996). This suggests that the source of the dust is in the south and that the dust is being washed out by the rain on its way northward.

2. Dynamics of the southern margins of the rain cloud system

Most of the rainfall in Israel is precipitated by convective clouds developing in cold air masses interacting

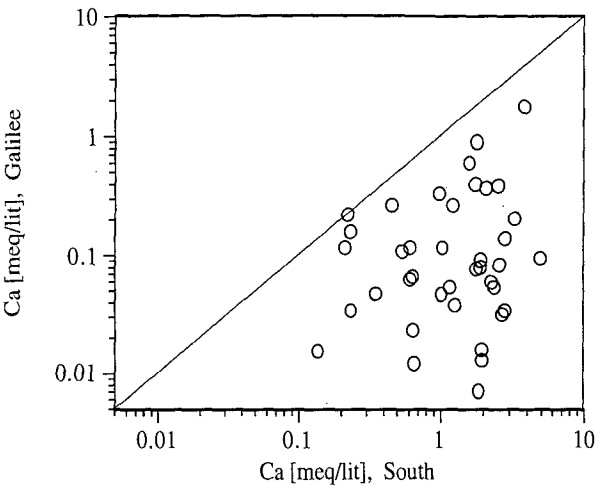

FIG. 3. Concentrations of calcium in rainwater (meq L^{-1}) occurring simultaneously in the south (northern and central Negev, Israel) and in the north (Galilee, Israel). The diagonal line denotes the 1:1 ratio.

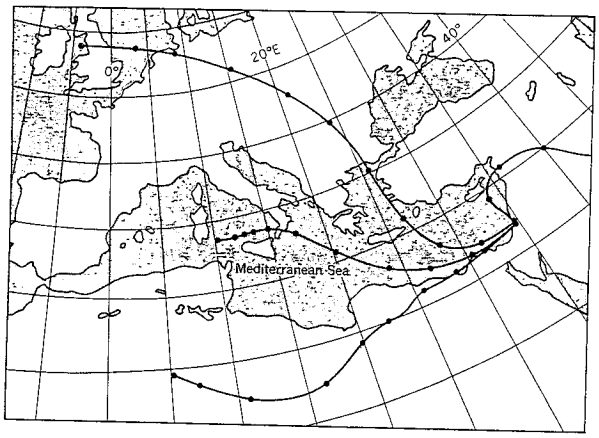

FIG. 4. Typical trajectories of air masses arriving at the Israeli Mediterranean coast on rainy days. The marked segments on the lines are 12-h intervals. The trajectories refer to the 850-mb level (about 1500 m) (after Gagin and Neumann 1974).

with the relatively warm water of the Mediterranean. The cold air flows typically from the Balkans southward through the Aegean Sea, curving cyclonically and arriving as mostly westerly flow to Israel (Shay-El and Alpert 1991). Rain clouds move inland to northern and central Israel with the westerly wind (Fig. 4). Due to the land–sea configuration, the back trajectory of the westerly wind that crosses southern Israel passes the North African and Sinai deserts. This air is much drier and cooler near the surface and, therefore, more stable than air with the more northerly maritime trajectory. The difference between the two flows is manifested in a sharp north–south gradient in the annual rain amounts just to the north of the latitude of the North African coastline.

Rain spells start typically with a cold front associated with a cyclone passing to the north. The front is typically oriented from northeast to southwest. Strong south to southwesterly winds very often blow desert dust into the frontal rainband, which constitutes the SMR.

Most of the rainfall in central Israel falls from the cold air mass behind the cold front. The SMR in the postfrontal cold air mass is often associated with a convective rainband, oriented from west to east (see a typical weather radar image in Fig. 5). The rain cells move along the rainband eastward, so that the position of the rainband remains nearly stationary, crossing the Israeli coastline typically near the latitude of Gaza. This rainband and the dynamical structure of the low-level flow in this situation are illustrated schematically in Fig. 6.

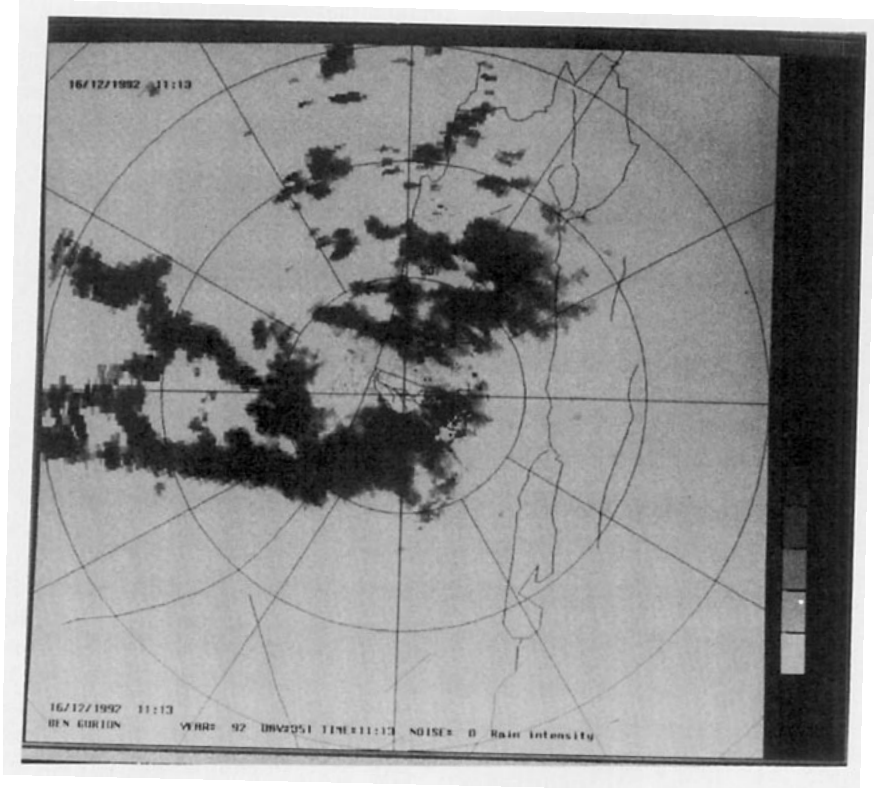

FIG. 5. A radar image of the precipitation reflectivity map during conditions of a North African coastal front. The radar is located at Ben-Gurion airport near Tel Aviv. The range circles are 50-km intervals.

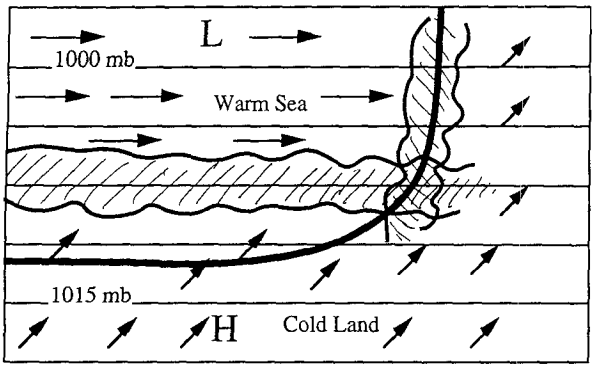

FIG. 6. Schematic illustration of the low-level flow during a typical rain situation in Israel.

This scheme is supported by modeling and observations presented in Khain et al. (1993). The elements constituting Fig. 6 are as follows.

- The location is the southeastern corner of the Mediterranean.
- The land is colder than the sea surface temperature.
- The air masses are colder than the sea surface temperature. There is a stable boundary layer over land and an unstable boundary layer over the sea.
- Geostrophic westerly winds occur above the boundary layer, parallel to the North African coastline.
- As a result of the colder air over land, a land breeze component develops and diverts the flow toward the sea.
- The large stability of the boundary layer air over land and the enhanced friction with the land surface slow down the air to a velocity smaller than that of a geostrophic equilibrium. The pressure gradient is no longer balanced by the Coriolis effect. Since the low pressure is to the north, the low-level southerly component over land is increased.
- The confluence of the low-level southwesterly flow from the land with the low-level westerly flow over the sea creates a convergence line in the sea parallel to the North African coast.
- Rain clouds develop over this convergence line and move eastward with the geostrophic flow above the boundary layer. The clouds cross the Israeli coast typically in the center of the southern target area of the Israel-3 rain enhancement experiment. This precipitation band constitutes the SMR, as mentioned above.
- The low-level air with continental trajectory is ingested into the North African coastal convergence line. The air, after absorbing heat and moisture from the sea, contributes to the formation of the SMR convective clouds.
- This continental air is often laden with desert dust that "seeds" the SMR clouds that ingest it.

This mechanism of coastal convergence was first recognized by Bergeron (1949). It was later described in New England by Bosart (1975), who named it the "coastal front." Further documentation of the coastal front was done in New England (Nielsen 1989; Nielsen and Neilley 1990) and Scandinavia (Okland 1990). This coastal front mechanism [type B coastal front, according to Nielsen (1989)] is also capable of injecting desert dust into the SMR in purely westerly to slightly northwesterly winds above the boundary layer, which seemingly have no trajectory over the North African and Sinai land areas, in accordance with the observations presented in Fig. 2. The North African coastal front is almost always manifested as a precipitation band in situations of polar outbreaks with 850-mb winds varying between 240° and 280° during the early and central winter months. The coastal front appears on the radar screen as a west–east rainband of convective clouds moving along the orientation of the band, parallel to the North African coastline in the sea. The width of the rain band is 10–40 km, averaging 30 km.

Much of the rainfall in the southern experimental area is contributed from the SMR, which is often organized as a coastal front. The important role of the coastal front in Israel is demonstrated in Fig. 7. This figure displays the amount of rainfall that fell from airmass convection away from cold and warm fronts or vorticity centers, as a percentage of the overall rain amount that was measured by radar during two full rain seasons (the winters of 1976/67 and 1977/78). According to Fig. 7, a distinct maximum of the rain amounts occurred at the approximate location of the coastal front, as schematically illustrated in Fig. 6.

3. Data and methodology

The impact of the desert dust and of the location of the SMR on the effectiveness of seeding is investigated for northern Israel. The analysis is based on data of daily rainfall amounts in the northern target and control areas (NT and NC in Fig. 1) and in the subareas of the southern target area SC, SN, and SS. The data include 330 unseeded days in the north in the winter seasons of 1963/64–1974/75 (of which 201 are in the Israel-2 period) and 1441 seeded days during the seasons 1969/70–1990/91 (226 in the Israel-2 period). Only rainy days with at least 0.1 mm of rain in the northern control area were included in the analysis. A fixed set of about 70 rain gauges in the north and 40 rain gauges in the south was used throughout the analysis.

The data were broken into four subgroups defined by two SMR locations (north and south) and two dust conditions (dust and no dust). The SMR was defined as being in the south if the average daily rainfall in SS (Fig. 1) exceeded 1 mm and otherwise as being in the north. Dust condition was defined by the dust index described in section 1f.

The statistical analysis is composed of two elements. First, seeding effects and confidence intervals are es-

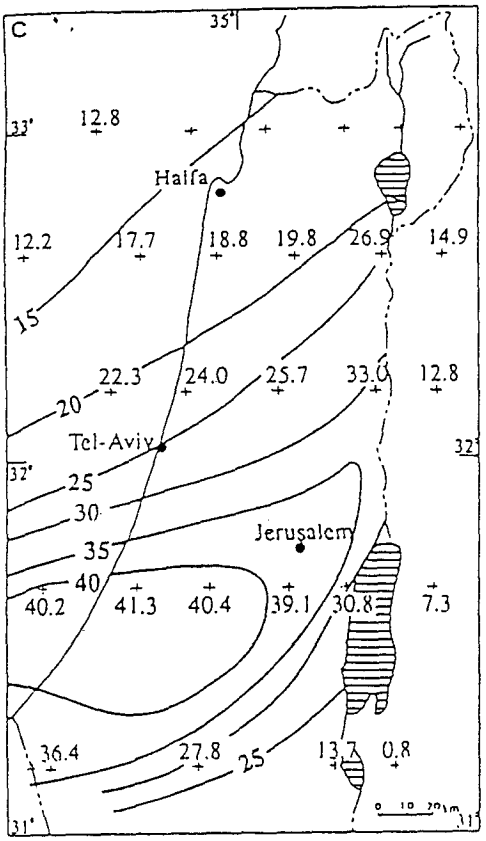

FIG. 7. The amount of rainfall that fell from airmass convection away from fronts or vorticity centers, as a percentage of the overall rain amount that was measured by radar during two full rain seasons (the winters of 1976/77 and 1977/78).

timated. Second, inference on the *differences* between effects in different subgroups is carried out.

In a recent paper by Nirel and Rosenfeld (1995), a method for estimating the seeding effect of the operational seeding was developed. The method is based on a historical model of target precipitation on control precipitation. The validity of such an approach stems from the stability of the relationship between target and control precipitation over time. The examination of the temporal variation of the model parameters and of relevant meteorological variables showed that there was no significant time trend in all series studied.

Seeding effects are estimated by the double ratio adjusted for historical regression (DRHR):

$$\mathrm{DRHR} = \frac{R_s}{R_u} = \left(\frac{\bar{Y}_s}{\hat{\bar{Y}}_s}\right)\left(\frac{\bar{Y}_u}{\hat{\bar{Y}}_u}\right)^{-1}, \qquad (1)$$

where $\bar{Y}_s$ is the mean rainfall in the target area on seeded days, $\bar{Y}_u$ is the mean rainfall in the target area on unseeded days, and $\hat{\bar{Y}}_s$ and $\hat{\bar{Y}}_u$ are defined similarly for the predicted rainfall in the target area.

A logarithmic regression model with a shift parameter is used to predict the logarithm of the target rainfall $\ln(y_i)$ by the logarithm of the control rainfall $\ln(x_i)$:

$$\ln(y_i + \mu) = \beta_0 + \beta_1 \ln(x_i + \mu) + \epsilon_i,$$
$$E(\epsilon_i) = 0, \quad \mathrm{var}(\epsilon_i) = \eta^2, \qquad (2)$$

where β_0 is the intercept, β_1 the slope, μ the shift parameter ($\mu = 0.3$ mm), and ϵ_i the error term with mean zero and variance η^2.

The estimated target rainfall in original scale is given by the replacement of the parameters by their estimates (denoted by hats) and the retransformation

$$\hat{y}_i = \exp(\hat{\beta}_0 + 0.5\,\hat{\eta}^2)(x_i + \hat{\mu})^{\hat{\beta}_1} - \hat{\mu}. \qquad (3)$$

Confidence intervals are constructed by the bootstrap method, since the number of days in subgroups is not large enough for approximation by the normal distribution. The bootstrap method consists of resampling for an estimation of the distribution of complex statistics such as double ratios (Efron and Gong 1983). It is based on a repeated sampling, *with replacement* from the dataset. A large number of samples is drawn, and an estimate of the double ratio is computed for each sample. The bootstrap distribution is constructed from the set of these estimates. Confidence intervals are derived from the percentiles of the bootstrap distribution. Nirel (1994) compared several bootstrap methods for construction of confidence intervals for DRHR and showed that the $1 - \alpha$ and level interval defined by the $\alpha/2$ and $1 - \alpha/2$ percentiles of the bootstrap distribution have the correct asymmetry. The bootstrap is based on the independence and equal distribution of the observations. Consecutive rainy days have a weak temporal dependence. However, when the data are broken into subgroups, the prevalence of consecutive rainy days is very small, and the bootstrap is valid.

Differences between effects are analyzed by two nonparametric tests. The first is for differences between two subgroups (dust versus no dust, north SMR versus south SMR). For each subgroup a set of 22 annual estimates (for each of the seasons 1969/70–1990/91) was computed. After independence of the two sets of estimates was verified, the Wilcoxon test for two independent samples was applied. The second test is for differences between four subgroups (a combination of dust index and SMR location). The Kruskal–Wallis test was used to identify overall differences. A simultaneous test was used for detection of the subgroups that contributed to the significant overall difference (Seigel and Castellan 1988).

4. The dependence of seeding effects on desert dust and location of the SMR

Analysis of the rain distribution in different dust and SMR conditions (Table 1) shows that the average daily rainfall on unseeded days in the north on dust and no-

TABLE 1. Rain distribution in the target and control areas by the dust index and the location of the SMR on seeded and unseeded days.

		Location of the SMR					
		North		South		All	
Area	Dust index	n (u) n (s)	Rain (mm)	n (u) n (s)	Rain (mm)	n (u) n (s)	Rain (mm)
Target	0	58	1.6	102	8.6	160	6.1
		323	2.5	560	8.4	883	6.2
	1	78	4.2	92	9.2	170	6.9
		248	3.7	310	12.2	558	8.4
	All	136	3.1	194	8.9	330	6.5
		571	3.0	870	9.7	1441	7.1
Control	0	58	2.2	102	10.5	160	7.5
		323	2.9	560	8.8	883	6.6
	1	78	3.8	92	9.1	170	6.7
		248	3.7	310	11.3	558	7.9
	All	136	3.2	194	9.8	330	7.1
		571	3.3	870	9.7	1441	7.1

dust days was similar (6.9 and 6.1 mm, respectively). The average daily rainfall was 8.9 mm on days with south SMR (59% of the days) and 3.1 mm on days with north SMR. The average amount for dust days with south SMR (28% of the days) was 9.2 mm and for a north SMR 4.1 mm (24% of the days). The lowest daily average (1.6 mm) was indicated on no-dust days with north SMR (18% of the days). Table 2 presents the effect estimates. For each combination of dust and SMR conditions, four estimates are given: all days (1969/70–1990/91), operational period only (1975/76–1990/91), and two estimates for the Israel-2 period. The first estimate for Israel-2 is based on seeded days in the period of 1969/70–1974/75, but the unseeded days are taken from the period of 1963/64–1974/75. The second estimate is based on both seeded and *unseeded* days in the Israel-2 period (1969/70–1974/75). The estimates and the respective 95% confidence interval for all days are also illustrated in Fig. 8.

Looking first at the margins of the table, it is seen that on days with the SMR at the south the indicated rain enhancement for all days reached 11% (significant), but when the SMR drifted northward the indicated effect was −8% (insignificant). The difference between these effects was found to be highly significant ($\alpha = 0.0004$). In 18 years out of the 22 years of available data, a larger seeding effect was detected on days with south SMR (Fig. 9).

Similar analysis for the two dust conditions indicated a significant increase of 13% in rain amounts on no-dust days and an insignificant effect of 6% on dust days. The difference between the seeding effects on dust and no-dust days had a significance level of $\alpha = 0.067$. The

TABLE 2. Seeding effects in the north (DRHR) and the corresponding 95% confidence intervals [$c(l)$, $c(u)$], stratified by the dust index and by the location of the SMR. Estimates in the first three rows in each cell are based on seeded days during (a) all days (1969/70–1990/91), (b) operational period (1975/76–1990/91), (c) Israel-2 period (1969/70–1974/75), and on unseeded days in the period 1963/64–1974/75. Estimates on the fourth row (noted by asterisk) correspond to both seeded and unseeded days of the Israel-2 period.

		South SMR			North SMR			All		
Dust index	Period	N	DRHR	[$c(l)$, $c(u)$]	N	DRHR	[$c(l)$, $c(u)$]	N	DRHR	[$c(l)$, $c(u)$]
No-dust	1970–91	662	1.13	[1.04, 1.26]	381	1.19	[0.90, 1.60]	1043	1.13	[1.04, 1.25]
	1976–91	586	1.11	[1.01, 1.23]	341	1.23	[0.91, 1.67]	927	1.12	[1.02, 1.23]
	1970–75	178	1.25	[1.11, 1.43]	98	0.99	[0.70, 1.40]	276	1.20	[1.06, 1.37]
	1970–75*	144	1.29	[1.13, 1.48]	78	1.17	[0.78, 1.71]	222	1.25	[1.09, 1.44]
Dust	1970–91	402	1.11	[0.96, 1.28]	326	0.89	[0.76, 1.09]	728	1.06	[0.94, 1.19]
	1976–91	335	1.11	[0.97, 1.29]	283	0.92	[0.78, 1.11]	618	1.06	[0.95, 1.20]
	1970–75	159	1.09	[0.90, 1.32]	121	0.73	[0.53, 0.98]	280	1.03	[0.88, 1.21]
	1970–75*	122	1.09	[0.88, 1.35]	83	0.68	[0.49, 0.91]	205	1.01	[0.85, 1.20]
All	1970–91	1064	1.11	[1.02, 1.22]	707	0.92	[0.80, 1.11]	1771	1.08	[1.00, 1.17]
	1976–91	921	1.10	[1.00, 1.21]	624	0.95	[0.81, 1.15]	1545	1.07	[0.99, 1.16]
	1970–75	337	1.18	[1.05, 1.33]	219	0.76	[0.60, 0.96]	556	1.11	[1.00, 1.23]
	1970–75*	266	1.20	[1.06, 1.37]	161	0.74	[0.57, 0.99]	427	1.12	[1.00, 1.27]

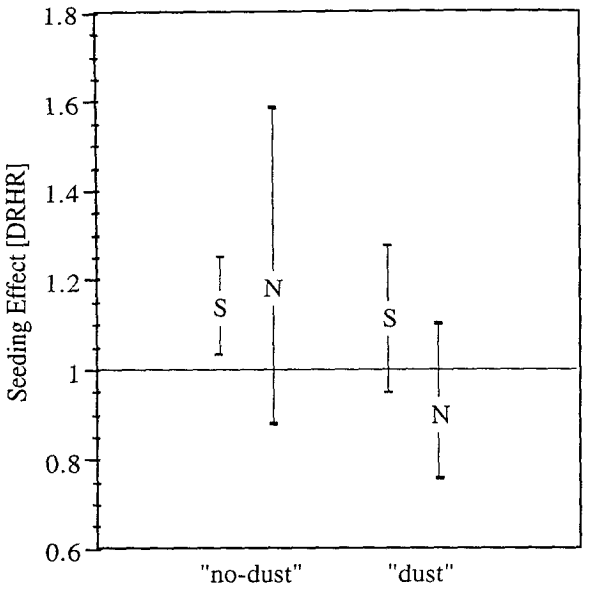

FIG. 8. Seeding effect in the north during the years 1969/70–1990/91, stratified by dust and no-dust days and by the location of the SMR. The values of the effects are at the center of the characters (N and S for north and south SMR, respectively). The lower and upper bounds of the 95% confidence interval are denoted by the vertical lines.

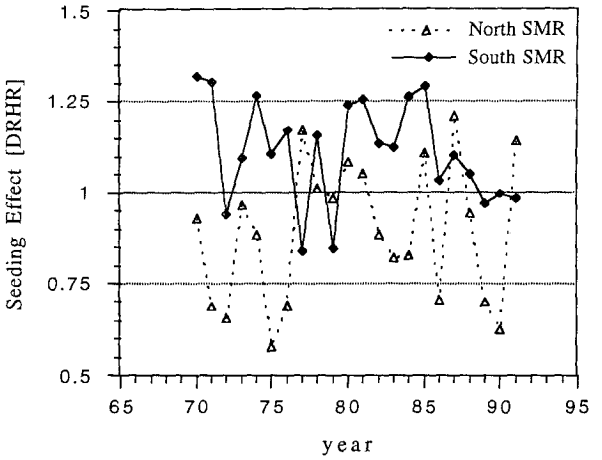

FIG. 9. Yearly seeding effect in the north during 1969/70–1990/91, stratified by the SMR location.

annual estimates (Fig. 10) point consistently to a larger effect on no-dust days.

Considering the interaction of the SMR location and the dust factor (the entries within Table 2), it is seen that on dust days the effects vary greatly with the location of the SMR. An insignificant effect of −11% is indicated on days with north SMR, and an insignificant enhancement of 11% on days with south SMR. On no-dust days both estimates are positive. On days with south SMR, when conditions are most favorable, significant effect of 13% and 19% is indicated on days with south and north SMR, respectively.

The test for overall difference between the four estimates was highly significant ($\alpha = 0.0003$). Pairwise tests indicated that the only significant comparisons accounting for the overall significance were those comparing the seeding effect on dust days with north SMR (least favorable condition) with the other three groups.

Comparison between the operational and the Israel-2 experiment periods indicates that the findings are consistent, though more extreme in the Israel-2 period. The effects for south SMR are 10% in the operational period and 18% in Israel-2, and for north SMR −5% and −24%, respectively. For dust days, the corresponding amounts are 11% and 9% on south SMR and −8% and −27% on north SMR. For no-dust days with south SMR the estimates are 11% in the operational period and 25% in the Israel-2 period. For the above cells, the Israel-2 estimates are insensitive to the change in the control period; that is, the estimates on the third and fourth rows of each cell are similar.

On no-dust days with north SMR the estimate are less homogeneous. The effect in the operational period is estimated by 23%, and the two Israel-2 estimates are −1% and 17%. The variability of estimates in the no-dust/north SMR conditions is also reflected by the long confidence interval on these days (see also Fig. 8). This variability can be explained by the "conflicting" conditions prevailing on these days, which affect rain enhancement in opposite directions.

These results suggest that there is an interaction between dust conditions and the location of SMR: the impact of the dust is seen to be detrimental to the effectiveness of seeding on days with north SMR.

These statistical results are compatible with the following physical considerations.

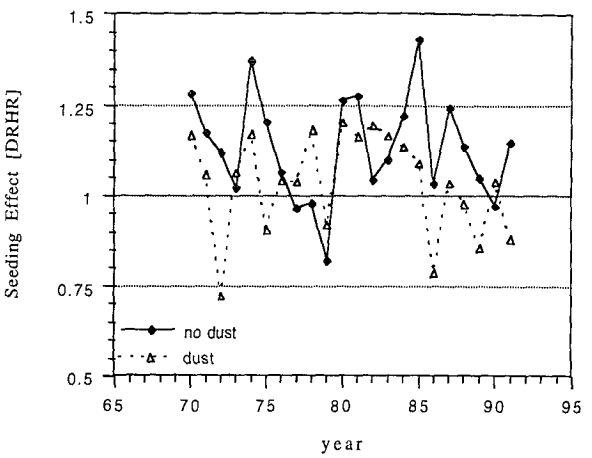

FIG. 10. Yearly seeding effect in the north during 1969/70–1990/91, stratified by dust and no-dust days.

- The strongest interaction of dust with rain clouds in the north occurs on dust days when the SMR is in the north.
- When the SMR moves to the south, much (but not all) of the dust can be washed down by the intervening rain between the north and the SMR.

5. Summary and conclusions

The southern margins of the rain cloud systems in Israel is constituted of rainbands of cold fronts and North African coastal fronts. The dynamic structure of the SMR is such that southerly low-level airflow is ingested into the convective clouds from their bases. This air is capable of "seeding" the clouds with desert dust. The desert dust is washed down by rain clouds to the north of the SMR.

Analyses of the seeding effects show that rain is enhanced in the north when the SMR is in the south. When the SMR is in the north, rain is enhanced only on days when no desert dust is observed. A physical mechanism for overseeding in the presence of dust is suggested. So far no factor other than the dust has been found to offer an alternative explanation to the north–south differences of the seeding effects in Israel.

Acknowledgments. This work was sponsored by EMS, a subsidiary of Mekoroth, the Israeli National Water Supply Company. The authors are grateful to the Israeli Meteorological Service for providing the data.

REFERENCES

Bergeron, T., 1949: The problem of artificial control of rainfall on the globe. II. The coastal orographic maxima of precipitation in autumn and winter. *Tellus,* **1,** 15–32.

Bosart, L. F., 1975: New England coastal frontogenesis. *Quart. J. Roy. Meteor. Soc.,* **101,** 957–978.

Efron, B., and G. Gong, 1983: A leisurely look at the bootstrap, the jackknife and cross validation. *Amer. Stat.,* **37,** 36–48.

Gabriel, R. K., and D. Rosenfeld, 1990: The second Israeli rainfall stimulation experiment: Analysis of precipitation on both targets. *J. Appl. Meteor.,* **29,** 1055–1067.

Gagin, A., 1965: Ice nuclei, their physical characteristics and possible effect on precipitation initiation. *Proc. Int. Conf. on Cloud Physics,* Tokyo and Sapporo, Japan, 155–162.

——, and J. Neumann, 1974: Rain stimulation and cloud physics in Israel. *Weather and Climate Modification,* W. N. Hess, Ed., Wiley-Interscience, 454–459.

——, and ——, 1981: The second Israeli randomized cloud seeding experiment: Evaluation of the results. *J. Appl. Meteor.,* **20,** 1301–1311.

Ganor, E., 1991: The composition of clay minerals transported to Israel as indicators of Saharan dust emission. *Atmos. Environ.,* **25A,** 2657–2664.

Hallet, J., and S. C. Mossop, 1974: Production of secondary particles during the rimming processes. *Nature,* **249,** 26–28.

Isono, K., M. Komabayasi, and A. Ono, 1959: The nature and the origin of ice nuclei in the atmosphere. *J. Meteor. Soc. Japan,* **37,** 211–233.

Khain, A. P., D. Rosenfeld, and I. Sednev, 1993: Coastal effects in the eastern Mediterranean as seen from experiments using a cloud ensemble model with detailed description and ice microphysical processes. *J. Atmos. Res.,* **30,** 295–319.

Levi, Y., and D. Rosenfeld, 1996: Ice nuclei, rainwater chemical composition, and static seeding effects in Israel. *J. Appl. Meteor.,* **35,** 1494–1501.

Levin, Z., C. Price, and E. Ganor, 1990: The contribution of sulfate and desert dust aerosols to the acidification of clouds and rain in Israel. *Atmos. Environ.,* **24A,** 1143–1151.

——, E. Ganor, and V. Gladstein, 1996a: The effects of desert particles coated with sulfate on rain formation in the eastern Mediterranean. *J. Appl. Meteor.,* **35,** 1511–1523.

——, S. Tzivion, and T. Reisin, 1996b: Rain production in convective clouds as simulated in an axisymmetric model with detailed microphysics. Part II: Effects of varying drops and ice initiation. *J. Atmos. Sci.,* **53,** 1815–1837.

Nielsen, J. W., 1989: The formation of New England coastal fronts. *Mon. Wea. Rev.,* **117,** 1380–1401.

——, and P. P. Neilley, 1990: The vertical structure of New England coastal fronts. *Mon. Wea. Rev.,* **118,** 1793–1807.

Nirel, R., 1994: Bootstrap confidence intervals for estimation of seeding effect in an operational period. *Statistics for the Environment II: Water-Related Issues,* V. Barnett and K. F. Turkman, Eds., John Wiley, 109–123.

——, and D. Rosenfeld, 1994: The third Israeli rain enhancement experiment—An intermediate analysis. *Proc. Sixth WMO Scientific Conf. on Weather Modification,* Paestum, Italy, World Meteor. Org., 569–572.

——, and ——, 1995: Estimation of the effect of operational seeding on rain amounts in Israel. *J. Appl. Meteor.,* **34,** 2220–2229.

Okland, H., 1990: The dynamics of coastal troughs and coastal fronts. *Tellus,* **42A,** 444–462.

Rosenfeld, D., and H. Farbstein, 1992: Possible influence of desert dust on seedability of clouds in Israel. *J. Appl. Meteor.,* **31,** 722–731.

Schaefer, V. J., 1949: The formation of ice crystals in the laboratory and the atmosphere. *Chem. Rev.,* **44,** 291.

——, 1954: The concentrations of ice nuclei in air passing the summit of Mt. Washington. *Bull. Amer. Meteor. Soc.,* **35,** 310–314.

Shay-El, Y., and P. Alpert, 1991: A diagnostic study of winter diabatic heating in the Mediterranean in relation with cyclones. *Quart. J. Roy. Meteor. Soc.,* **117,** 715–747.

Siegel, S., and N. J. Castellan Jr., 1988: *Nonparametric Statistics for the Behavioral Sciences.* 2d ed. McGraw-Hill, 399 pp.